Electronic Supplementary Material (ESI) for Journal of Materials Chemistry A.

Supplementary Information

Intrinsically Stretchable Symmetric Organic Battery Based on Plant-Derived Redox Molecules

Nara Kim, Samuel Lienemann, Ziyauddin Khan, Grzegorz Greczynski, Aiman Rahmanudin, Mikhail Vagin, Fareed Ahmed, Ioannis Petsagkourakis, Jesper Edberg, Xavier Crispin*, and Klas Tybrandt**

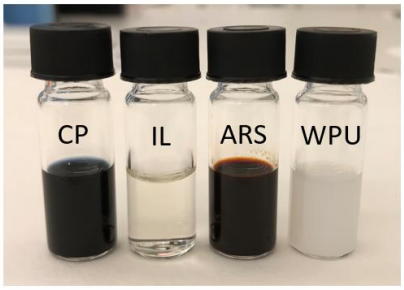

Fig. S1. Photographs of aqueous solutions and dispersions of the four constituent organic materials.

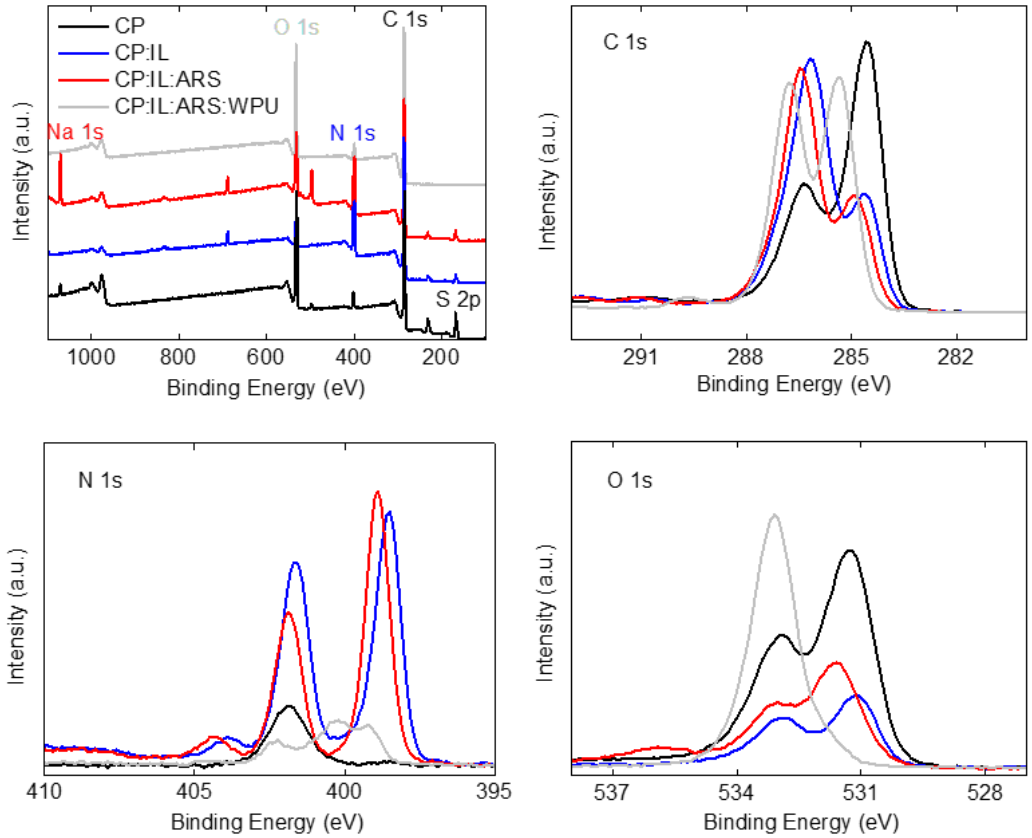

Fig. S2. XPS survey spectra and high resolution spectra of the C 1s, N 1s, and O 1s regions for CP and the composites when each component is added.

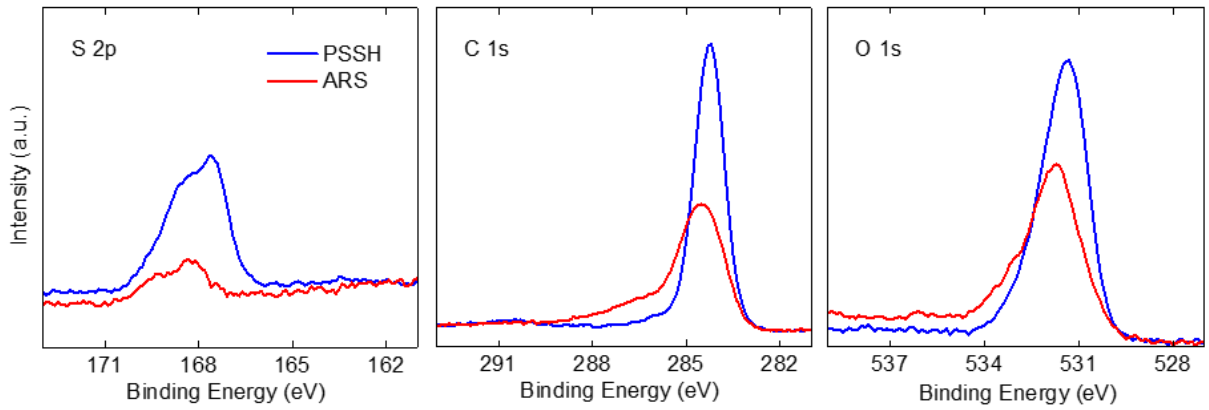

Fig. S3. High resolution XPS spectra of the S 2p, C 1s, and O 1s regions for PSSH and ARS.

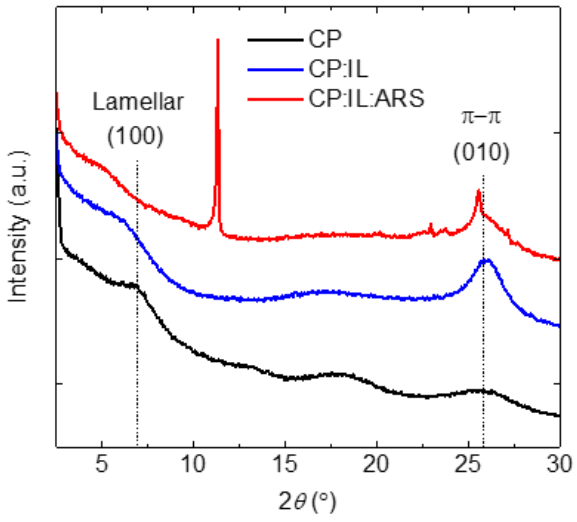

Fig. S4. XRD patterns of CP and the composites. Diffraction peaks denoted by (100) and (010) originate from the lamellar packing distance of PEDOT:PSS and the π-π stacking distance between PEDOT rings, respectively. [1] The peak shift towards a higher [lower] angle indicates a decrease [increase] in stacking distance. A sharp peak at 2θ=11.3° observed for the CP:IL:ARS composite film may come from ARS crystallites.

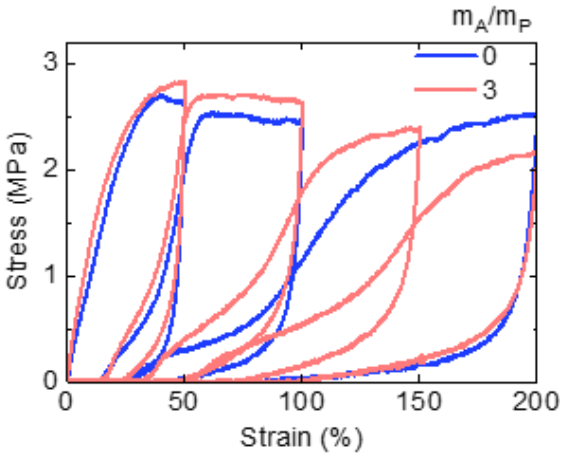

Fig. S5. Stress-strain curves of the composite (m_A/m_p=3) upon cyclic loading. Stress-strain curves of the CP:IL:ARS composite (m_A/m_p=0) is shown for comparison.

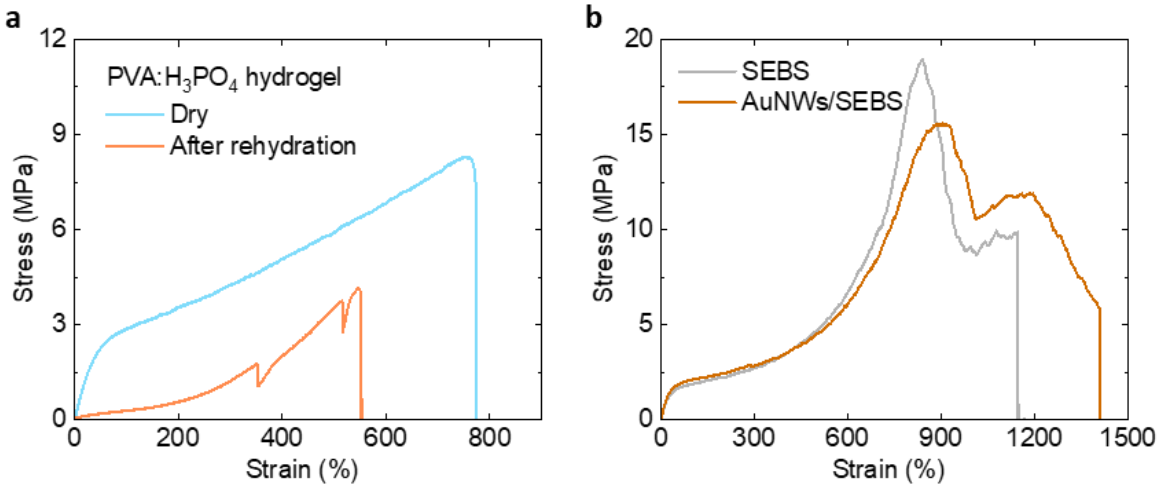

Fig. S6. (a) Stress-strain curves of dry PVA:H_3PO_4 hydrogel before (ca. 12 wt% water content) and after rehydration (ca. 45 wt% water content) with an aquoues ARS solution. PVA:H_3PO_4 hydrogel becomes much softer and sticky after rehydration. (b) Stress-strain curves of SEBS substrates with and without AuNW current collectors embedded in.

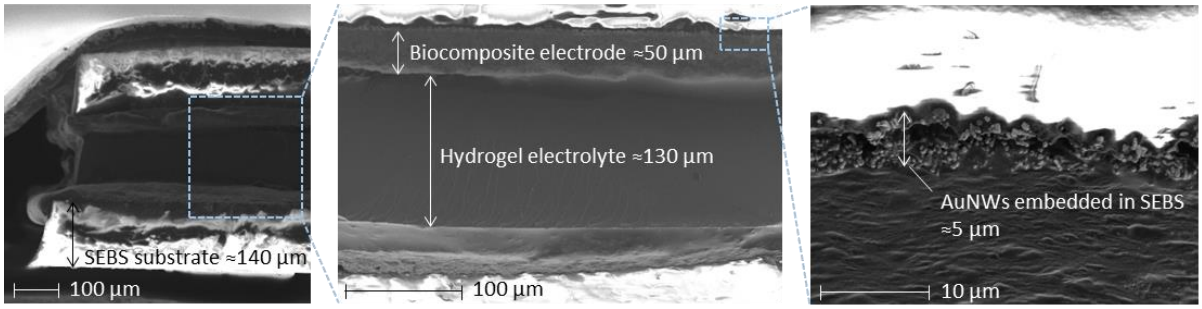

Fig. S7. Cross-sectional SEM images of the organic battery at various magnifications.

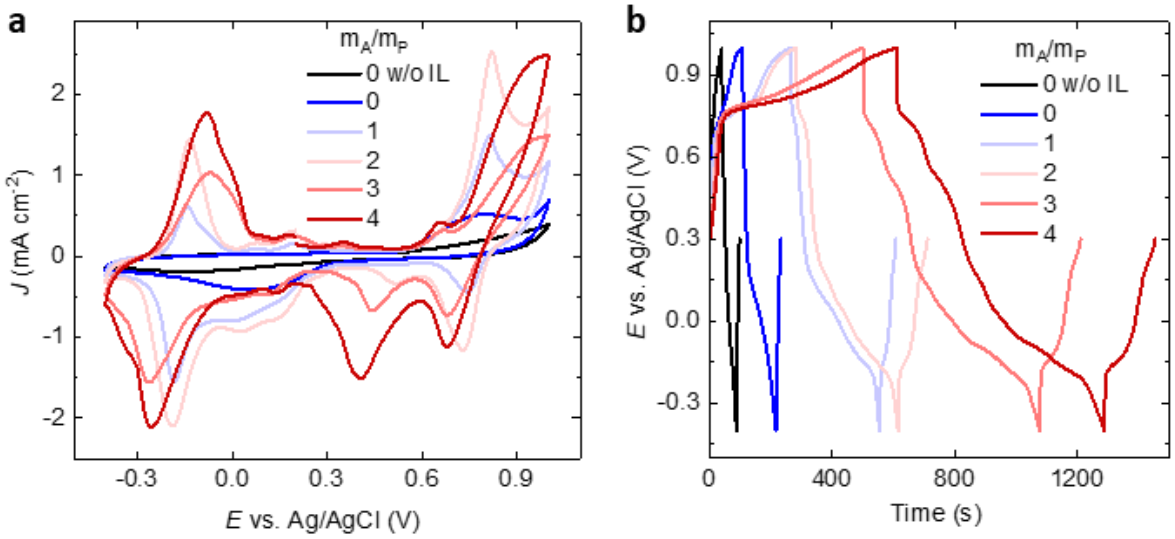

Fig. S8. (A) CV and (B) GCD characteristics of the CP:IL:ARS:WPU composite electrodes (i.e., the half-cell) with varying amount of ARS in a three-electrode measurement.

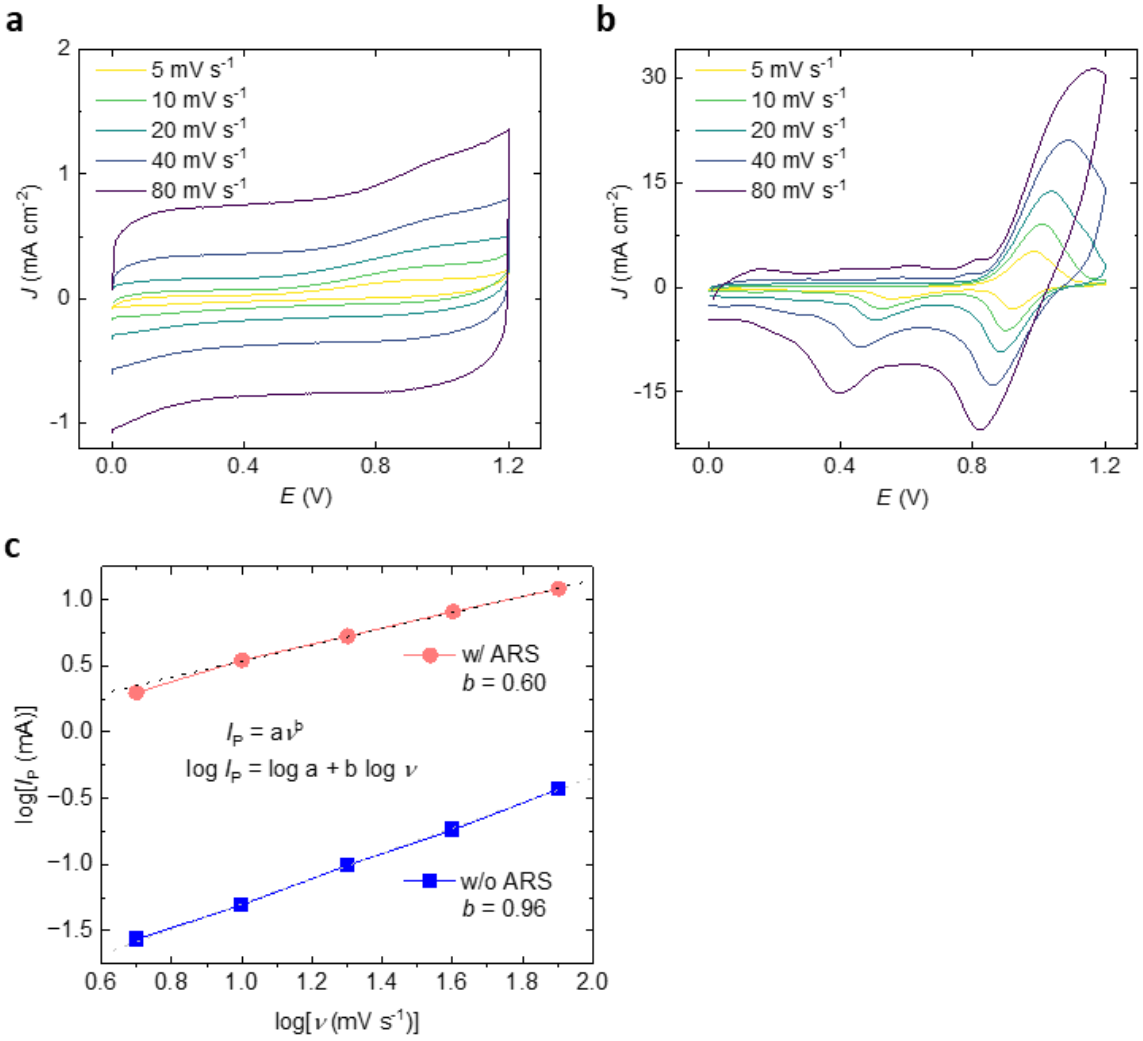

Fig. S9. CV of the devices (b) with and (a) without ARS measured at different voltage scan rates. (c) Relationship between cathodic peak current (I_P) and scan rate (ν). Since CV of the device withour ARS has a slightly slanted rectangular shape without an apparent peak, the values of cathodic current at 0.6 V were used to plot. The index b in the power law $I_P = a\nu^b$ is used as an indicator to distinguish different charge storage kinetics: diffusion-controlled process if b is close to 0.5; and surface-controlled process if b is close to 1. In this log plot, a slope corresponds to the b value.

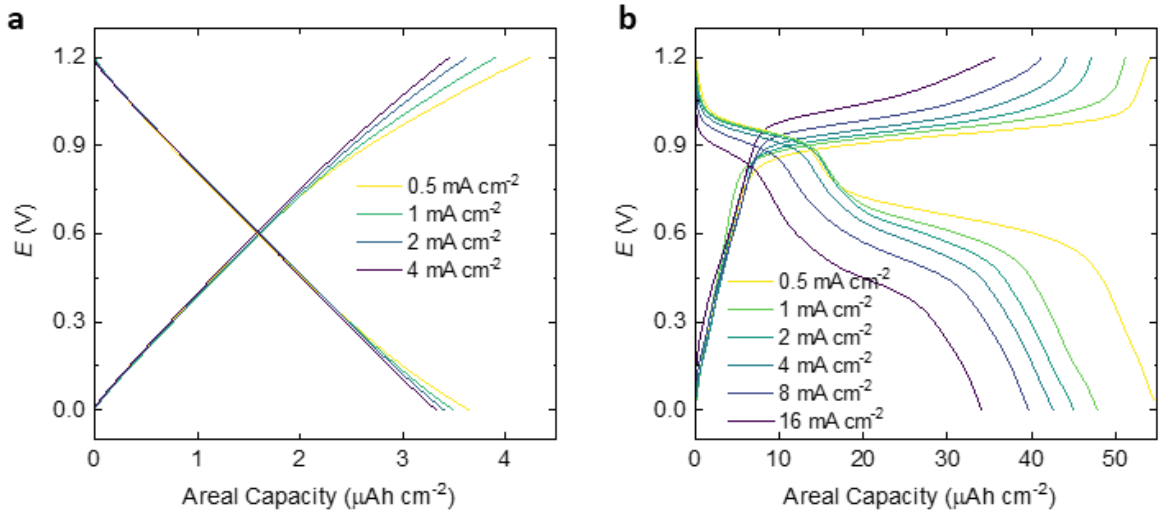

Fig. S10. GCD curves of the devices (b) with and (a) without ARS measured at different current densities.

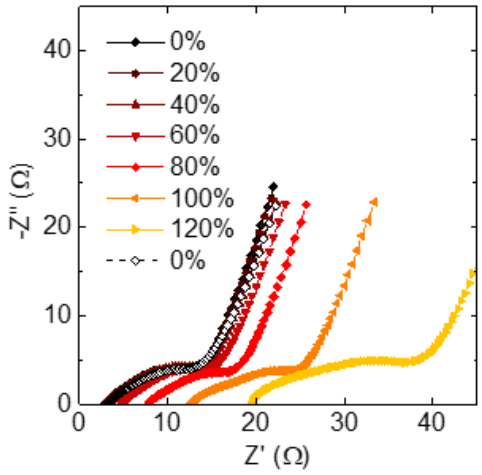

Fig. S11. Nyquist plots of the organic battery at various tensile strain.

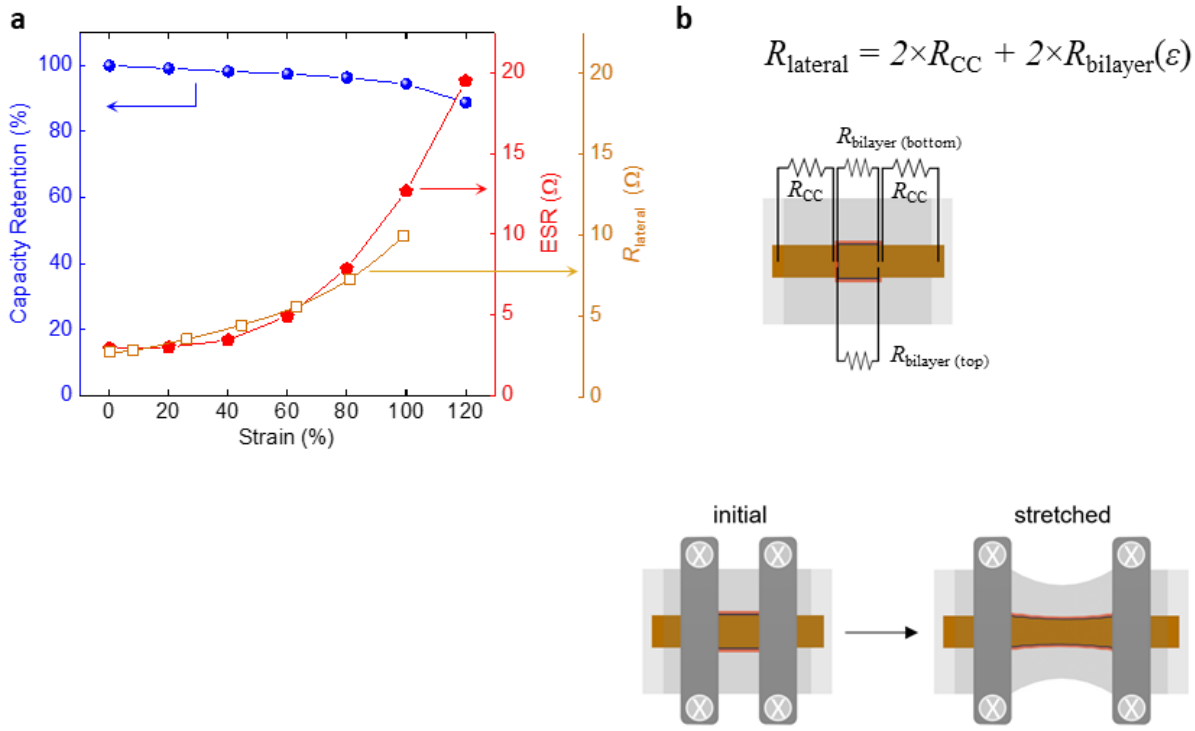

Fig. S12. (a) Capacity retention and ESR change of the organic battery under different tensile strains. (b) A lateral resistance ($R_{lateral}$) of the device was estimated from the presented equation. R_{CC} is the lateral R of AuNW current collector (CC) clamped on a linear stretching stage. $R_{bilayer}$ is the lateral R of the AuNW CC/biocomposite electrode bilayer as a fucntion of strain (ε), which is plotted in Fig. 3c.

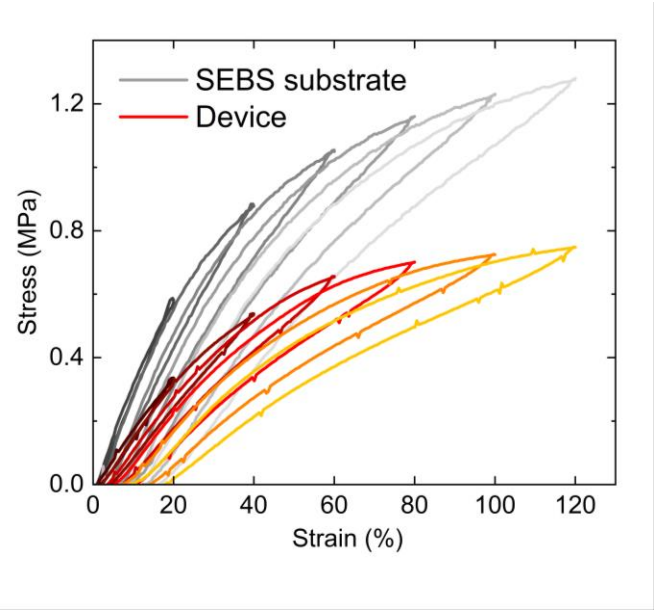

Fig. S13. Stress-strain curves of the organic battery device and a SEBS substrate upon cyclic strain loading at various levels (20-120%).

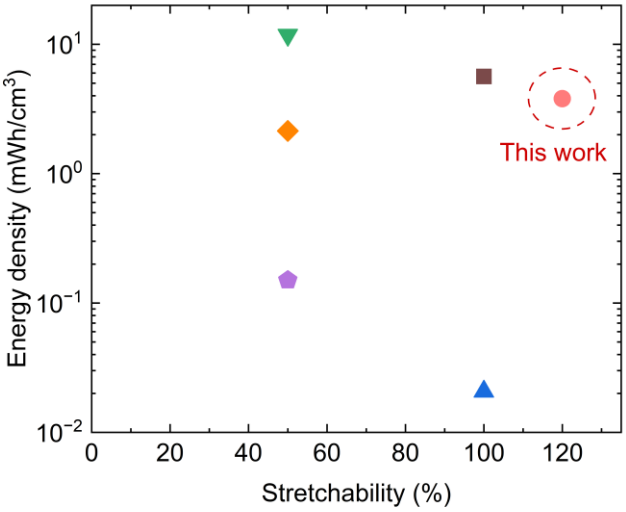

Fig. S14. Comparison of volumetric energy density and stretchability of the organic battery in this work with those of other intrinsically stretchable organic electrochemical energy storage devices in the literatures. Electrode materials: PEDOT NFs@FKM & PDAA@Ag NWs/FKM

(▼),[2] PU/carbon black/MWCNT (■),[3] PVA/PMAA/PEDOT:PSS (▲),[4] ACM/MWCNTs @PDAA & ACM/MWCNTs@PANI (◆),[5] and PANI/MWCNT/PDMS (⬟).[6]

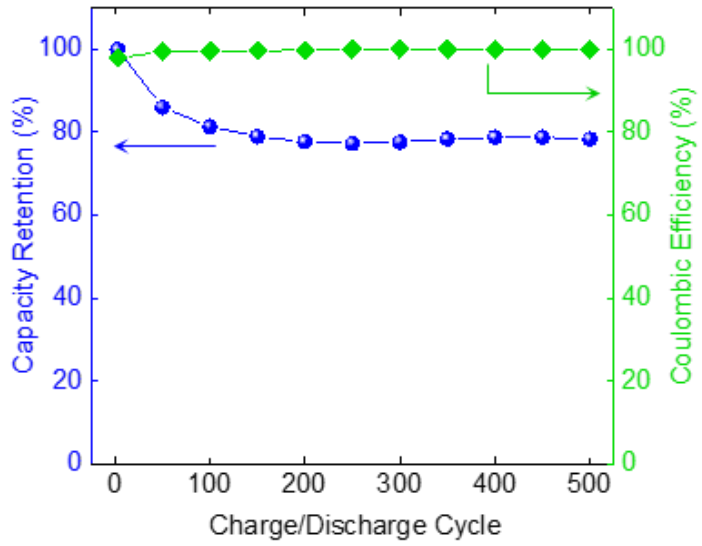

Fig. S15. Capacity retention and coulombic efficiency of the organic battery upon GCD cylces at 4 mA cm^{-2}.

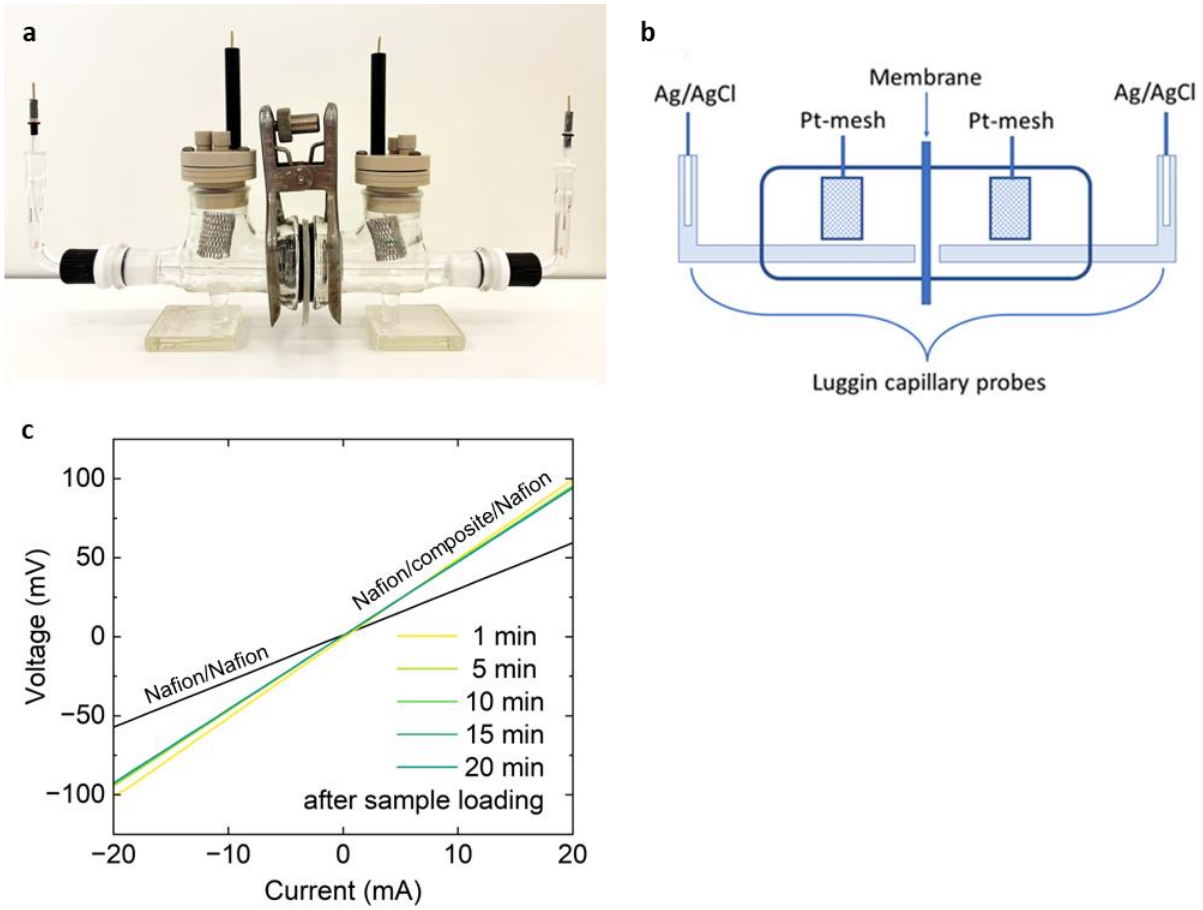

Fig. S16. (a) Photograph and (b) schematic of the H-cell used to measure ionic conductivity (σ_{ion}) of the composites. Reproduced with the permission from ref. [7]. The H-cell was filled with 4M H_3PO_4 as an electrolyte while Luggin capillary probes were filled with 3M KCl as salt bridge and capped with Ag/AgCl (3M KCl) reference electrodes. The capillary openings of the Luggin probes were positioned close to the membrane (≈2 mm from both sides of the membrane) and the position was kept the same throughout all measurements. (c) The measured resistance of the drop-cast CP:IL:ARS:WPU composite film decreases overtime after being placed in the H-cell set-up (i.e., immersed in electrolyte). Thus, the measurement was done 20−30 min after the sample loading when the resistance was stabilized.

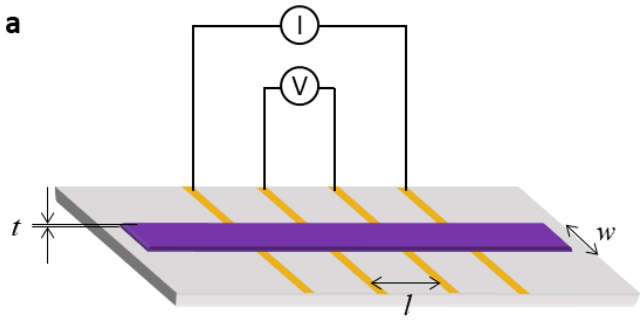

b

$$R = \mathrm{V/I} = \rho \times \mathrm{Area/Length} = \rho \times (w \times t)/l$$

$$\sigma_{dc} = 1/\rho = \mathrm{I/V} \times (w \times t)/l$$

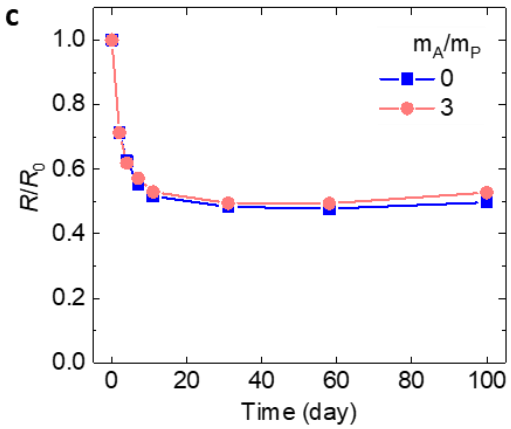

Fig. S17. (a) A four-lead geometry used to measure electrical dc conductivity (σ_{dc}) of the composites. Four yellow lines represent four Au lines deposited on a glass substrate. A purple strip represent a composite film attached on the substrate. *l* is the distance between the inner two Au lines. *w* and *t* are the width and thickness of a sample strip. Typical dimensions used in this study: *l*≈5 mm, *w*≈2 mm, *t*≈40 μm. (b) Equations to calculate σ_{dc} from measured resistance (*R*) and dimensions. ρ is the resistivity. (c) *R* of the drop-cast CP:IL:ARS:WPU composite film is decreasing over time and stabilized after a month. The initial *R* is higher due to the partial dedoping of PEDOT by NH_3 added to the composite solution to prevent acid-induced aggregation of the anionic WPU.[8] The doping level is recovered over time via spontaneous oxidation upon oxygen (air) exposure.[8] σ_{dc} in Fig. 2c was calculated from the stabilized *R* that was measured two months after the film preparation.

References

1. N. Kim, B. H. Lee, D. Choi, G. Kim, H. Kim, J.-R. Kim, J. Lee, Y. H. Kahng and K. Lee, *Phys. Rev. Lett.*, 2012, **109**, 106405.
2. H. Mu, W. Wang, L. Yang, J. Chen, X. Li, Y. Yuan, X. Tian, G. Wang, *Energy Storage Mater.*, 2021, **39**, 130–138
3. H. Mu, X. Huang, W. Wang, X. Tian, Z. An, and G. Wang, *ACS Appl. Mater. Interfaces*, 2022, **14**, 622−632
4. C.-C. Shih, Y.-C. Lina, M. Gaoa, M. Wua, H.-C. Hsieha, N.-L. Wu, W.-C. Chen, *J. Power Sources*, 2019, **426**, 205–215
5. X. Wang, C. Yang, J. Jin, X. Li, Q. Cheng and G. Wang, *J. Mater. Chem. A,* 2018, **6**, 4432-4442
6. M. Yu, Y. Zhang, Y. Zeng, M.-S. Balogun, K. Mai, Z. Zhang, X. Lu, and Y. Tong, *Adv. Mater.*, 2014, **26**, 4724–4729
7. S. Lander, M. Vagin, V. Gueskine, J. Erlandsson, Y. Boissard, L. Korhonen, M. Berggren, L. Wågberg and X. Crispin, *Adv. Energy Sustainability Res.*, 2022, **3**, 2200016.
8. N. Kim, S. Lienemann, I. Petsagkourakis, D. Alemu Mengistie, S. Kee, T. Ederth, V. Gueskine, P. Leclère, R. Lazzaroni, X. Crispin and K. Tybrandt, *Nat. Commun.*, 2020, **11**, 1424.